Conjugated Polymer Nanoparticles for Drug Delivery and Imaging

Xuli Feng, Fengting Lv, Libing Liu,* Hongwei Tang, Chengfen Xing, Qiong Yang, and Shu Wang*

Beijing National Laboratory for Molecular Sciences, Key Laboratory of Organic Solids, Institute of Chemistry, Chinese Academy of Sciences, Beijing 100190, P. R. China

ABSTRACT We prepared a new conjugated polymer nanoparticle with the size of about 50 nm that is prepared by electrostatic assembly of cationic conjugated polymer PFO and anionic poly(L-glutamic acid) conjugated with anticancer drug doxorubicin (PFO/PG-Dox). The PFO exhibits good fluorescence quantum yield, photostability, and little cytotoxicity to meet the essential requests for cell imaging. In PFO/PG-Dox nanoparticles, the fluorescence of PFO is highly quenched by Dox by electron transfer mechanism, and thus the PFO is in the fluorescence "turn-off' state. After PFO/PG-Dox nanoparticles are exposed to carboxypeptidase or are taken up by cancer cells, the poly(L-glutamic acid) is hydrolysed to release the Dox, inducing the activation of PFO fluorescence to "turn-on" state. This multifunctional nanoparticle system can deliver Dox to targeted cancer cells and monitor the Dox release based on fluorescence "turn-on" signal of PFO, which concurrently images the cancer cells. The present work opens the door for new functional studies of conjugated polymer in simultaneous imaging and disease therapeutics.

KEYWORDS: conjugated polymers • nanoparticles • imaging • drug delivery

INTRODUCTION

Up to date, chemotherapy based on anticancer drugs remains as one of the most effective treatments for a range of neoplasms (1). However, the high efficacy of anticancer drugs is associated with high systemic toxicity to normal cells and healthy tissue. As a way to circumvent the limitation, several targeted anticancer drug delivery systems have been developed, such as polymeric systems (2), liposomes (1b, 3), and inorganic nanoparticles (4). The polymer-based delivery systems where anticancer drugs are chemically encapsulated by covalent linking to polymers have attracted much attention because of their biocompatible, nonimmunogenic, biodegradable nature and controlled drug release into targeted cancer cells or tumor tissues (5). Furthermore, polymer−drug conjugates can facilitate higher drug payloads, lower systemic toxicity, prolong drug circulation time, and improve drug solubility and targeting (6). In this respect, negatively charged poly(L-glutamic acid) is an ideal drug carrier, and several poly(L-glutamic acid)−drug conjugates have been developed and used in various stages of clinical trials (7).

Biomedical imaging provides a tool for noninvasive and real-time monitoring of drug delivery to tumors in vivo, which is an ideal goal of chemotherapy treatment (8). In recent years, there has been great interest in the development of multifunctional therapeutic systems that integrate drugs, molecular targeting, and imaging agents (e.g., fluorescent dyes and magnetic resonance imaging agents) within one system (2, 4, 9). The simultaneous imaging and therapeutic capabilities of these systems is advantageous over conventional chemotherapy in improving the therapeutic outcome of drug therapy (10). Because the fluorescence technique is one of the most useful analytical tools in bioanalysis and imaging (11), multifunctional polymer systems have been widely used to monitor the delivery and release of anticancer drugs by loading or labeling polymeric delivery with appropriate fluorescent imaging agents (12). Typical fluorescent imaging agents include organic fluorescent dyes (13), silica nanoparticles (14), and quantum dots (QDs) (15). Fluorescent dyes often suffer from photobleaching and celluar toxicity (16). Although QDs have superior brightness and photostability, they are cytotoxic by leaching harmful metals from their nanocrystal core (17). These facts provide the motivation for designing new fluorescent materials for fluorescence imaging. One promising strategy is the development of fluorescent conjugated polymer materials that have established themselves as useful sensitively sesning platforms because of the signal amplification by a collective system response (18−20). Very recently, several conjugated polymers have been prepared for live-cell imaging because of their high fluorescence brightness, good photostability, and lower toxicity (21). Herein, we report a novel and simple electrostatic complex of positively charged conjugated polymer (PFO) and negatively charged poly(L-glutamic acid) conjugated with the model anticancer drug doxorubicin (PFO/PG-Dox, see Scheme 1). The conjugated polymer PFO exhibits good fluorescence quantum yield, photostability and little cytotoxicity that are the essential requests for cell imaging. The PFO/PG-Dox complex forms nanoparticles in water that can image cell, deliver Dox to

* Corresponding author. E-mail: wangshu@iccas.ac.cn (S.W.); liulibing@iccas.ac.cn (L.L.).
Received for review May 18, 2010 and accepted July 27, 2010

DOI: 10.1021/am100435k

Scheme 1. (a) Schematic Illustration of PFO/PG-Dox Complex System, Where the Fluorescence of PFO Is Highly Quenched by Dox Resulting in the Fluorescence "Turn-Off" State; Chemical Structures of PG-Dox Conjugate and PFO Are Also Shown; (b) Schematic Representation of Uptake of the Electrostatic Complex into Cancer Cells; Hydrolysis of Poly(L-glutamic acid) by Hydrolase in Lysosome Releases the Dox to Induce the Activation of PFO Fluorescence to "Turn-On" State, Thereby Sensing the Intracellular Delivery of Dox and Simultaneously Achieving Fluorescent Imaging; (c) Synthetic Routine of Cationic Conjugated Polymer PFO

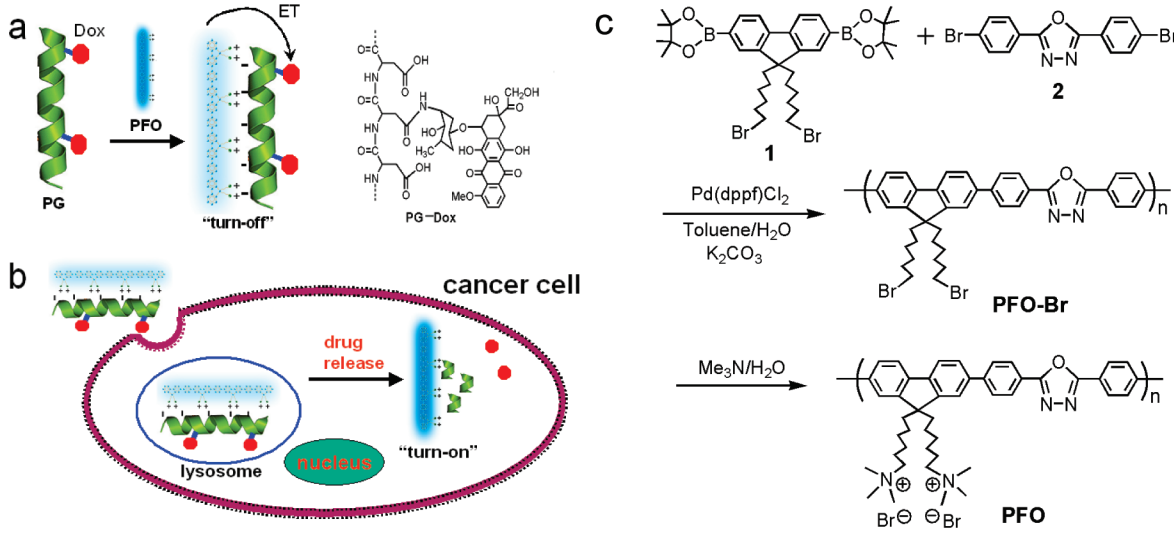

lung cancer (A549) cell and monitor the Dox release on the basis of fluorescence "turn-on" signal of PFO.

RESULTS AND DISCUSSION

As illustrated in Scheme 1a, the PFO/PG-Dox complex is composed of three components: (i) conjugated polymer PFO for fluorescence imaging; (ii) poly(L-glutamic acid) as drug carrier that is degraded by hydrolase in lysosome to release the covalent linking drug (7); (iii) Dox, which is one of the most effective chemotherapeutic anticancer drugs for various of neoplasms. The Dox contains one quinone group that is a highly efficient electron-transfer quencher (22). For PFO/PG-Dox complex, the fluorescence of PFO is highly quenched by Dox, and thus the PFO is in the fluorescence "turn-off" state. After PFO/PG-Dox complex is taken up by targeted cancer cells, the poly(L-glutamic acid) is hydrolysed to release the Dox. At this case, the Dox is far away from the PFO and the fluorescence of PFO is recovered, which induces the activation of PFO fluorescence to "turn-on" state (Scheme 1b). This multifunctional complex system can deliver Dox to targeted cancer cells and monitor the Dox release based on fluorescence "turn-on" signal of PFO, which concurrently images the cancer cells.

The synthesis of PFO is illustrated in Scheme 1c. Suzuki coupling reaction of equal equivalent of boronic ester **1** and compound **2** in the presence of 2.0 M aqueous K_2CO_3 and $Pd(dppf)Cl_2$ in toluene affords precursor polymer PFO-Br. The gel permeation chromatography (GPC) analyses show that the weight-average molecular weight (M_w) and number-average molecular weight (M_n) of PFO-Br are 10280 and 7190, respectively, with the polydispersity index (PDI) of 1.43. The PFO-Br is treated with excessive trimethylamine in THF to yield cationic conjugated polymer PFO.

The photophysical property of PFO was investigated in water. As shown in Figure 1a, the absorption spectrum of PFO exhibits a maximum peak at 378 nm with the extinction coefficient of $2.54 \times 10^4\ M^{-1}\ cm^{-1}$. Upon excitation at 380 nm, the emission spectrum shows a maximum peak at 454 nm. The PFO exhibits bright fluorescence in water with a quantum yield of 24%. The photostability of PFO was studied under strong UV irradiation by a mercury lamp (100

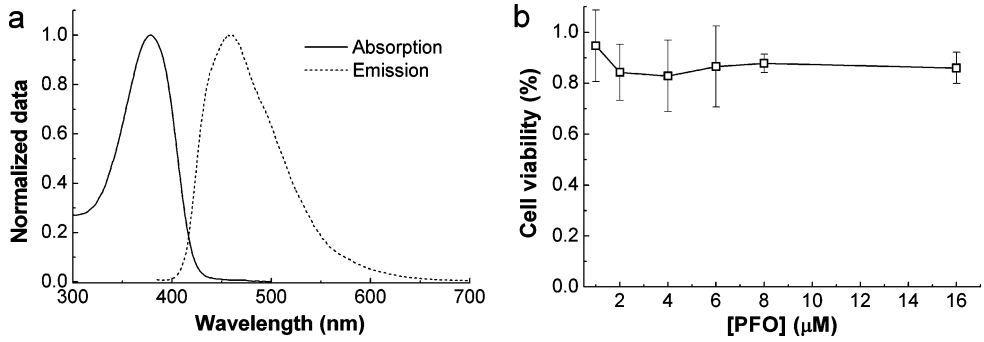

FIGURE 1. (a) Absorption and emission spectra of PFO in water. The excitation wavelength is 380 nm. (b) Cell viability results after incubation of A549 cells with various concentrations of PFO.

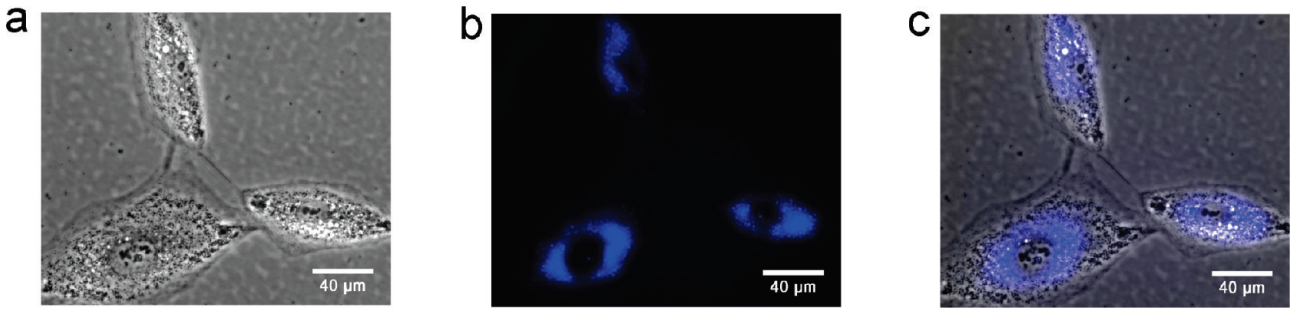

FIGURE 2. Cell imaging using PFO: (a) phase contrast image; (b) fluorescence image; (c) the overlap image of phase contrast and fluorescence of A549 cells treated with PFO. Fluorescence image was recorded on fluorescence microscopy (Olympus 1 × 71) using a 380/30 nm excitation filter with 100 ms exposure time.

W). The PFO fluorescence remains 60% upon continuously irradiating at 380 nm for 30 s. Our previous study showed that the fluorescence of representative dye fluorescein quickly droped below undetectable level in only 5 s upon irradiation by a mercury lamp (100 W) at 480 nm (18c). Electron-poor heterocyclic oxadiazole moiety in polymer backbone may be responsible for the good photostability of PFO because it can improve the electron transport and/or stability of polymers (23). The cytotoxicity of PFO was assayed using MTT method in which the conversion of soluble MTT into formazan is directly related to mitochondrial activity and subsequently to cell viability (24). Figure 1b shows the quantitative effect of PFO on cell viability. The cell viability decreases very less after 24 h incubation of lung cancer A549 cells with various concentrations of PFO (0−16 μM). The lower toxicity of PFO is critical for its imaging application. It is noted that most quantum dots and organic dyes such as fluoresceins, rhodamines, and cyanine dyes exhibit substantial cytotoxicity (16, 17).

On the basis of the lower cytotoxicity and good fluorescence performance of PFO, we applied this conjugated polymer for A549 cell imaging. Figure 2 shows the phase contrast image, fluorescence image and the overlap image of phase contrast and fluorescence of A549 cells that was treated with PFO (1 μM in repeated units (RUs)) at 37 °C for 4 h. From the fluorescence image, we can see that this conjugated polymer mainly locates in cytoplasm, especially around the perinuclear region and hardly enters nucleus. Thus, we can conclude that the PFO has crossed cell membranes to the interior of cells and concurrently imaged the cancer cells.

For drug delivery and imaging applications, we prepared the electrostatic complex of positively charged PFO with negatively charged PG-Dox conjugate. The polymer PG-Dox was synthesized by reacting poly(L-glutamic acid) with Dox in the presence of 1-ethyl-3-(3-dimethylaminopropyl) carbodiimide hydrochloride (EDC) (2c). The polymer of PG-Dox was purified by dialysis using membrane with molecular cutoff of 3500 for two days. The weight content of Dox in PG-Dox complex was assayed by absorption spectra to be about 10%. Poly(L-glutamic acid) was selected because of its biocompatible, nonimmunogenic, and biodegradable nature (7). The microstructural characterization of PFO/PG-Dox complex was performed by scanning electron microscope (SEM). As shown in Figure 3a, b, the PFO/PG-Dox complex forms nanoparticles in water with the size of about 50 nm, although the nanoparticles adhere to each other instead of dispersing well. As an initial step to validate that the fluorescence recovery of PFO can be applied for monitoring drug release, the PFO/PG-Dox complex was subjected to in vitro degradation under the conditions resembling those inside living cells. The subcellular lysosomal compartments (endosomes and lysosomes) of tumor cells often have reducing environments and possess several hydrolytic enzymes at acidic pH (pH ≤5.8) (25). Therefore, we exposed the complex to carboxypeptidase at 37 °C in phosphate buffer (100 mM, pH 5.8) that can cleave the amide bonds of poly(L-glutamic acid). As shown in Figure 3c, the PFO itself emits strong fluorescence in phosphate buffer. For PFO/PG-Dox complex, the fluorescence of PFO is efficiently quenched because of the electron transfer from PFO to Dox. Upon adding carboxypeptidase and allowing to incubate for 24 h, about 80% fluorescence of PFO is recovered because of the hydrolysis of poly(L-glutamic acid) that makes the quencher Dox far away from PFO.

To determine the drug release efficiency at various time intervals, we first examined the Stern−Volmer constant (K_{sv}) by monitoring measurable fluorescence changes of PFO using Stern−Volmer eq , where F_0 and F are the emission intensity of PFO in the absence and presence of the quencher Dox, respectively, and [Q] is the concentration of the quencher Dox (26).

$$F_0/F = 1 + K_{sv}[Q] \quad (1)$$

As shown in Figure 4a, the fluorescence of PFO is gradually quenched as additions of PG-Dox. A linear Stern−Volmer plot is obtained with a K_{sv} value of 1.12×10^8 M^{-1} (Figure 4b). For PFO/PG-Dox complex in the presence of carboxypeptidase, the concentration of Dox can be calculated from the fluorescence intensity of PFO from the Stern−Volmer curve to calculate the drug release efficiency. As shown in Figure 4c, the anticancer drug Dox is released quickly at the first six hours and gradually reaches a plateau after 24 h. Thus we can monitor the Dox release quantitatively based on the fluorescence "turn-on" signal of PFO using PFO/PG-Dox complex.

The results obtained from in vitro Dox release studies motivated us to further investigate the uptake of PFO/PG-

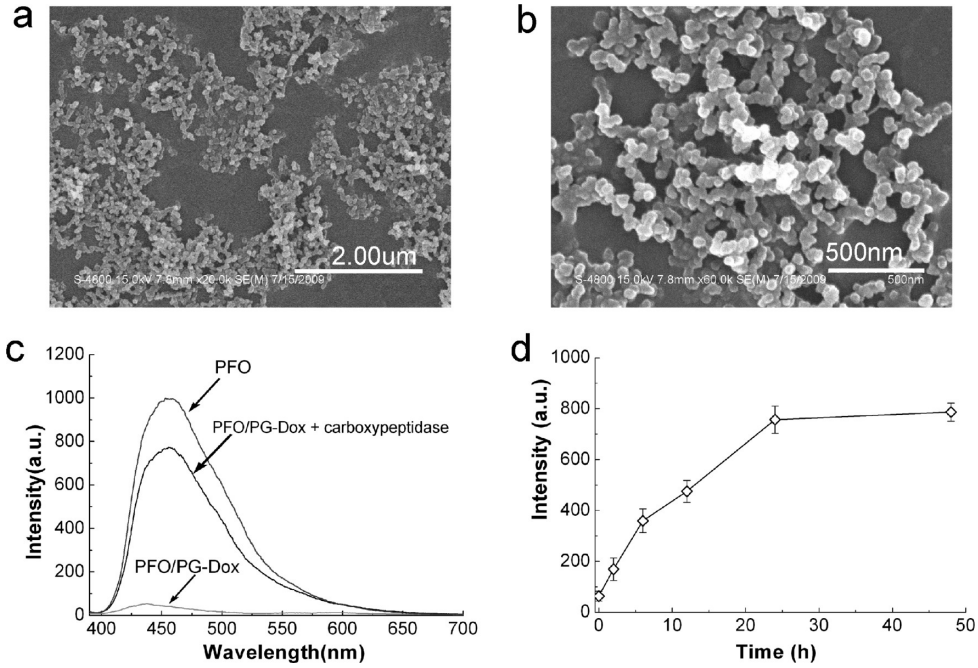

FIGURE 3. (a) Lower- and (b) higher-magnification SEM images of PFO/PG-Dox complex. (c) Emission spectra of PFO, PFO/PG-Dox complex before and after treatment with carboxypeptidase for 24 h. (d) Fluorescence intensity of PFO/PG-Dox complex at 454 nm as a function of carboxypeptidase incubation time. The measurements are performed in phosphate buffer (100 mM, pH= 5.8). [PFO] = 1.0×10^{-6} M in RUs, [Dox] = 1.03×10^{-7} M, 0.5 U of carboxypeptidase. The excitation wavelength is 380 nm. The error bars represent the standard deviation of three measurements.

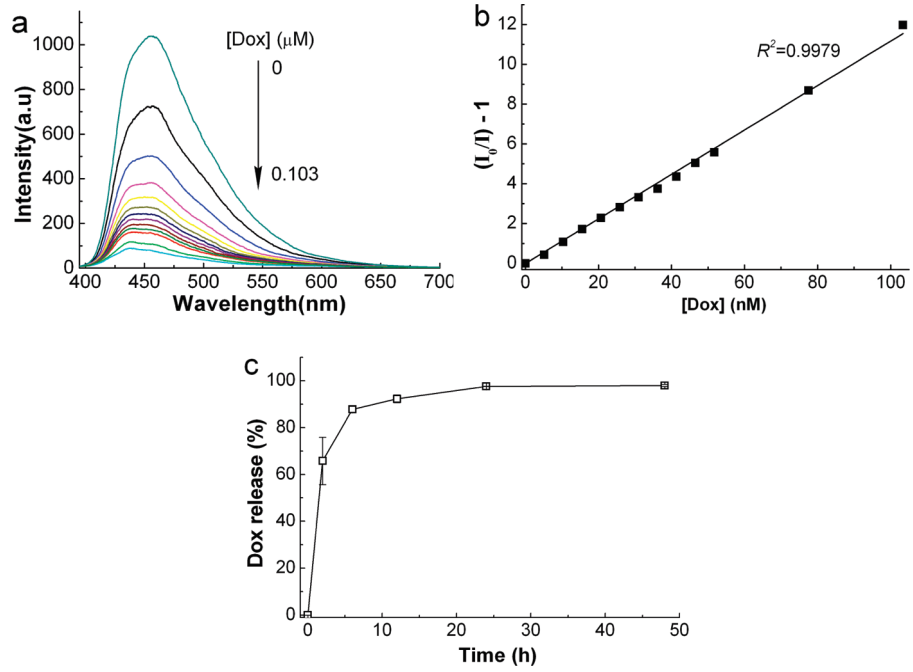

FIGURE 4. (a) Fluorescence emission spectra of PFO with successive additions of PG-Dox. (b) K_{sv} plot of PFO in the presence of PG-Dox. [PFO] = 1.0×10^{-6} M in RUs, [Dox] = $0-1.03 \times 10^{-7}$ M. (c) Drug release profiles at various time intervals after adding carboxypeptidase. [PFO] = 1.0×10^{-6} M in RUs, [Dox] = 1.03×10^{-7} M, 0.5 U of carboxypeptidase. Fluorescence measurements were performed in phosphate buffer (100 mM, pH 5.8) with excitation wavelength of 380 nm.

Dox complex into A549 cells and monitor the Dox release in cells by fluorescence microscopy. In this experiment, A549 cells were incubated with PFO/PG-Dox complex at 37 °C for 4 h and washed twice using PBS buffer to remove free PFO/PG-Dox complex, and then the cells were imaged after further incubation for certain times prior to fluorescence imaging. As shown in Figure 5, with 0 h further incubation, the fluorescence of PFO was less observed (Figure 5a, middle), whereas the fluorescence of Dox was clearly observed (Figure 5a, right). These observations exhibited the PFO/PG-Dox complex uptaked into cells and the PFO remained largely in "turn-off" state. After 24h further incubation, bright blue fluorescence of PFO was observed inside the cells (Figure 5b, right) because of more Dox release from

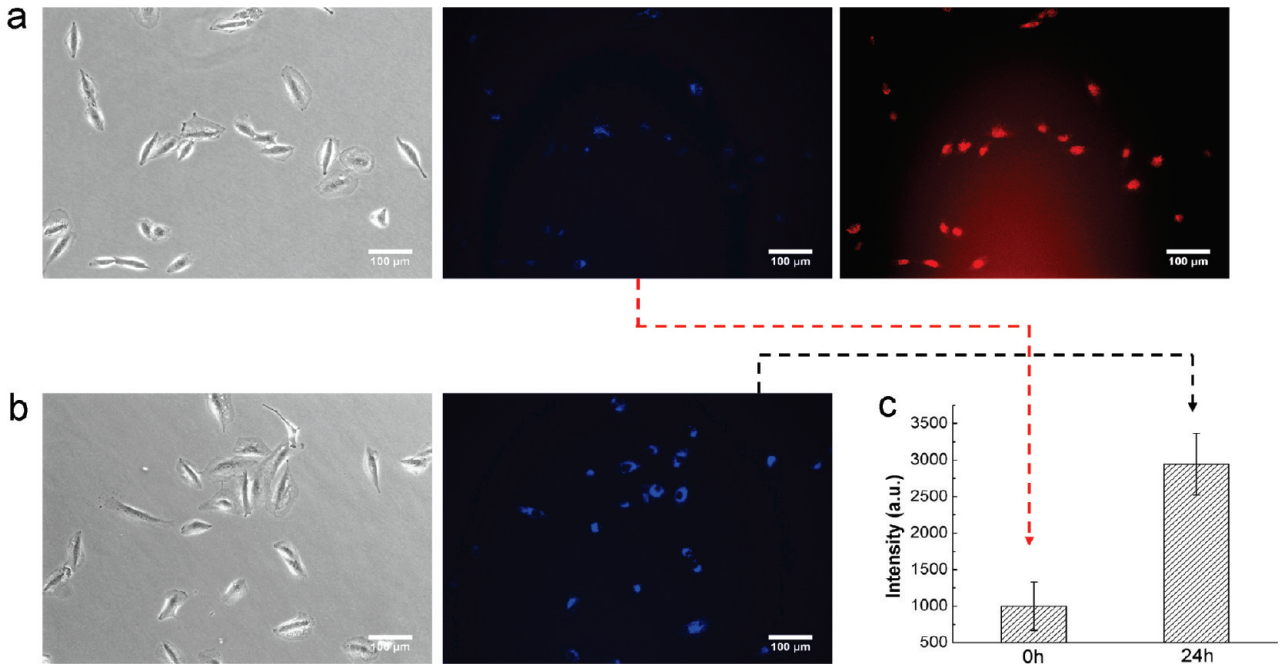

FIGURE 5. Microscopy images of A549 cells after incubation with PFO/PG-Dox complex for 4 h at 37 °C, washed two times with PBS buffer, and further incubated at 37 °C for (a) 0 and (b) 24 h. PFO and Dox are shown in blue and red, respectively. (c) The fluorescence recovery of PFO in the cells with Dox release. [PFO] = 1.0×10^{-6} M in RUs, [PG-Dox] = 3.35×10^{-6} M. Fluorescence image of PFO was recorded by fluorescence microscopy (Olympus 1×71) using a 380/30 nm excitation filter with 200 ms exposure time and that of Dox was recorded using a 455/70 nm excitation filter with 1000 ms exposure time.

the complex in lysosome, showing the "turn-on" state of PFO/PG-Dox complex. At this case, the weak fluorescence of Dox was also observed. Thus, we can monitor the drug release process by observing the fluorescence recovery of PFO (Figure 5c). Therefore, the multifunctional PFO/PG-Dox complex system can deliver Dox to targeted cancer cells and monitor the Dox release based on fluorescence "turn-on" signal of PFO, which concurrently images the cancer cells. It is noted that the PFO and the PFO/PG-Dox complex both enter the cell via endocytosis mechanism.

CONCLUSIONS

In summary, a new fluorescent cationic polyfluorene containing oxadiazole moieties (PFO) has been prepared and characterized for live-cell imaging. It exhibits high fluorescence brightness, good photostability, and little cytotoxicity. The PFO can form electrostatic complex with negatively charged poly(L-glutamic acid) conjugated with anticancer drug doxorubicin (PFO/PG-Dox). The PFO/PG-Dox complex forms nanoparticles in water with the size of about 50 nm. This multifunctional complex system can deliver Dox to targeted cancer cells and monitor the Dox release based on fluorescence "turn-on" signal of PFO, which concurrently images the cancer cells. The present work initiates new biological application of conjugated polymers and opens the door for new functional studies of conjugated polymer in simultaneous imaging and disease therapeutics.

EXPERIMENTAL SECTION

Materials and Measurements. All chemicals were purchased from Alfa Aesar or Acros and used as received if not specially stated. Compound **1** (27) and **2** (28) were prepared according to reported procedures. Water was purified using a Millipore filtration system. The ^{1}H NMR spectra were recorded on an AV 400 spectrometer. The gel permeation chromatography (GPC) measurement was performed on a Water-410 system against polystyrene standards with tetrahydrofuran (THF) as eluent. UV−vis absorption spectra were taken on a JASCO V-550 spectrophotometer or the absorbance was recorded on a microplate reader (BIO-TEK Synergy HT, USA). Fluorescence emission spectra were recorded at room temperature with Hitiachi F-4500 fluorescence spectrophotometer with a Xenon lamp as excitation source. SEM images were taken on Hitachi S-4800 scanning electron microscopy. Phase contrast bright-field and fluorescence images were taken with fluorescence microscopy (Olympus 1×71) with a mercury lamp (100 W) as light source.

Synthesis of Polymer PFO-Br. To a mixture of compound **1** (100 mg, 0.134 mmol) and **2** (85.2 mg, 0.134 mmol) in 4 mL of toluene and 2 mL of 2 M K_2CO_3 was added $PdCl_2$(dppf) (15 mg) under a nitrogen atmosphere. The resulting mixture was stirred at 80 °C for 2 days under nitrogen. After the mixture was cooled to room temperature, chloroform was added and the mixture was washed with water three times. The organic layer was dried over anhydrous $MgSO_4$ and the solvent was removed, and then the residue was added into acetone to precipitate the product. The crude polymer was purified by precipitation from chloroform into acetone twice and dried under vacuum to afford yellow solids. ^{1}H NMR (400 MHz, $CDCl_3$): δ 8.30−8.26 (m, 3H), 7.90−7.88 (m, 8H), 7.72−7.67 (m, 5H), 3.29 (s, 4H), 2.13 (s, 4H), 1.69 (s, 4H), 1.20 (d, 8H), 0.78 (s, 4H). GPC: M_n = 7190, M_w = 10280, PDI = 1.43.

Synthesis of Polymer PFO. To a solution of PFO-Br (20 mg) in tetrahydrofuran (THF) was added 10-fold excessive trimethylamine, and the mixture was stirred overnight at room temperature. Excessive trimethylamine and the solvent were removed under vacuum to afford yellow solids. ^{1}H NMR (400 MHz, DMSO): δ 8.30 (s, 3H), 8.11 - 8.00 (m, 8H), 7.87 (s, 5H), 3.84 (s, 4H), 3.09 (s, 18H), 2.95 (s, 4H), 2.11 (m, 4H), 1.50 (s, 4H), 1.07 (s, 4H), 0.7 (s, 4H).

MTT Assay. A549 cells were seeded in 96-well tissue culture plates in a 5% CO_2 humidified atmosphere and maintained overnight in DMEM medium. The PFO with varying concentrations were respectively added into the cells followed by further culture for 24 h at 37 °C. The culture media were discarded and MTT (1 mg/mL, 100 μL/well) was added to the wells, followed by incubation at 37 °C for 4 h. The supernatant was abandoned, and 150 μL of DMSO per well was added to dissolve the produced formazan and the plates were shaken for an additional 10 min, and the absorbance of the purple formazan was recorded on microplate reader (BIO-TEK Synergy HT, USA) at a wavelength of 520 nm.

Dox Release In vitro. To a solution of PFO/PG-Dox complex ([PFO] = 1.0×10^{-6} M, [PG-Dox] = 3.35×10^{-6} M) in 100 mM PBS buffer (pH 5.8) was added 0.5 U carboxypeptidase, then the solution was incubated at 37 °C for a certain period of time (from 0 to 48 h). The fluorescence intensity of PFO at 454 nm was measured at various time intervals with the excitation wavelength of 380 nm. The fluorescence intensity of PFO was converted into the concentration of Dox using Stern−Volmer curve to calculate the drug release efficiency.

Cell Imaging. One microliter of 1.0 mM PFO was added into 1 mL of DMEM medium containing A549 cells in 35 × 35 mm plate (the final concentration of PFO in medium is 1.0 μM). The plate was incubated at 37 °C for 8 h, then the medium was removed. The cells were washed with phosphate-buffered saline (PBS, pH 7.4) for two times before taking image. The fluorescent images were recorded on fluorescence microscopy (Olympus 1 × 71) using a 380/30 nm excitation filter with 100 ms exposure time.

Dox Release in Living Cell. A549 cells were seeded onto 35 × 35 mm culture plates and incubated at 37 °C in a 5% CO_2 humidified atmosphere for 24 h. The PFO/PG-Dox complex was added to the cells followed by further incubation at 37 °C for 4 h. The medium was removed and the cells were washed two times with PBS buffer. The cells were further incubated at 37 °C for a certain period of time, and then the images of PFO or Dox were recorded by fluorescence microscopy (Olympus 1 × 71). Fluorescence image of PFO was recorded using a 380/30 nm excitation filter with 200 ms exposure time and that of Dox was recorded using a 455/70 nm excitation filter with 1000 ms exposure time.

Acknowledgment. This work is supported by the National Natural Science Foundation of China (20725308, 90913014 and TRR61) and the Major Research Plan of China (2006CB932100).

REFERENCES AND NOTES

(1) (a) Minotti, G.; Menna, P.; Salvatorelli, E.; Cairo, G.; Gianni, L. *Pharmacol. Rev.* **2004**, *56*, 185–229. (b) Ewesuedo, R. B.; Ratain, M. J. In *Principles of Cancer Chemotherapy*; Vokes, E. E., Golomb, H. M., Eds.; Oncologic Therapeutics, Springer: New York, 2003, pp 19−66. (c) Shi, M.; Ho, K.; Keating, A.; Shoichet, M. S. *Adv. Funct. Mater.* **2009**, *19*, 1689–1696.

(2) (a) Nasongkla, N.; Bey, E.; Ren, J.; Ai, H.; Khemtong, C.; Guthi, J. S.; Chin, S.-F.; Sherry, A. D.; Bothman, D. A.; Gao, J. *Nano Lett.* **2006**, *6*, 2427–2430. (b) Lu, Z.-R.; Ye, F.; Vaidya, A. *J. Controlled Release* **2007**, *122*, 269–277. (c) Wang, L. L.; Wu, Y. X.; Xu, R. W.; Wu, G. Y.; Yang, W. T. *Chi. J. Polym. Sci.* **2008**, *26*, 383–391. (d) Medina, S. H.; El-Sayed, M. E. H. *Chem. Rev.* **2009**, *109*, 3141–3157.

(3) (a) Petros, R. A.; Ropp, P. A.; DeSimone, J. M. *J. Am. Chem. Soc.* **2008**, *130*, 5008–5009. (b) Ferrara, K. W.; Borden, M. A.; Zhang, H. *Acc. Chem. Res.* **2009**, *42*, 881–892.

(4) (a) Liong, M.; Lu, J.; Kovochich, M.; Xia, T.; Ruehm, S. G.; Nel, A. E.; Tamanoi, F.; Zink, J. I. *ACS Nano* **2008**, *2*, 889–896. (b) Kim, J.; Piao, Y.; Hyeon, T. *Chem. Soc. Rev.* **2009**, *38*, 372–390. (c) Morgan, T. T.; Muddana, H. S.; Altinoğlu, E. I.; Rouse, S. M.; Tabakoviæ, A.; Tabouillot, T.; Russin, T. J.; Shanmugavelandy, S. S.; Butler, P.; Eklund, P. C.; Yun, J. K.; Kester, M.; Adair, J. H. *Nano Lett.* **2008**, *8*, 4108–4115.

(5) (a) Haag, R.; Kratz, F. *Angew. Chem., Int. Ed.* **2006**, *45*, 1198–1215. (b) Maeda, H.; Seymour, L. W.; Miyamoto, Y. *Bioconjugate Chem.* **1992**, *3*, 351–362.

(6) (a) Ye, F.; Ke, T.; Jeong, E.-K.; Wang, X.; Sun, Y.; Johnson, M.; Lu, Z.-R. *Mol. Pharm.* **2006**, *3*, 507–515. (b) Godwin, A.; Bolina, K.; Clochard, M.; Dinand, E.; Rankin, S.; Simic, S.; Brocchini, S. *J. Pharm. Pharmacol.* **2001**, *53*, 1175–1184.

(7) (a) Bhatt, R.; Vries, P.; Tulinsky, J.; Bellamy, G.; Baker, B.; Singer, J. W.; Klein, P. *J. Med. Chem.* **2003**, *46*, 190–193. (b) Auzenne, E.; Donato, N. J.; Li, C.; Leroux, E.; Proce, R. E.; Farquhar, D.; Klostergaard, J. *Clin. Cancer Res.* **2002**, *8*, 573–581.

(8) (a) Rudin, M.; Weissleder, R. *Nat. Rev. Drug Discovery* **2003**, *2*, 123–131. (b) Mulder, W. J. M.; Strijkers, G. J.; Van Tilborg, G. A. F.; Cormode, D. P.; Fayad, Z. A.; Nicolay, K. *Acc. Chem. Res.* **2009**, *42*, 904–914.

(9) (a) Viglianti, B. L. *Abdom. Imaging* **2009**, *34*, 686–695. (b) Bagalkot, V.; Zhang, L. F.; Levy-Nissenbaum, E.; Jon, S. Y.; Kantoff, P. W.; Langer, R.; Farokhzad, O. C. *Nano Lett.* **2007**, *7*, 3065–3070. (c) Nehilla, B. J.; Allen, P. G.; Desai, T. A. *ACS Nano* **2008**, *2*, 538–544.

(10) (a) Domaille, D. W.; Que, E. L.; Chang, C. J. *Nat. Chem. Biol.* **2008**, *4*, 168–175. (b) Johnsson, N.; Johnsson, K. *ACS Chem. Biol.* **2007**, *2*, 31–38. (c) De, M.; Ghosh, P. S.; Rotello, V. M. *Adv. Mater.* **2008**, *20*, 4225–4241. (d) Dhar, S.; Daniel, W. L.; Giljohann, D. A.; Mirkin, C. A.; Lippard, S. J. *J. Am. Chem. Soc.* **2009**, *131*, 14652–14653.

(11) (a) Giepmans, B. N. G.; Adams, S. R.; Ellisman, M. H.; Tsien, R. Y. *Science* **2006**, *312*, 217–224. (b) Alivisatos, A. P.; Gu, W. W.; Larabell, C. *Annu. Rev. Biomed. Eng.* **2005**, *7*, 55–76.

(12) (a) Kim, J.; Lee, J. E.; Lee, S. H.; Yu, J. H.; Lee, J. H.; Park, T. G.; Hyeon, T. *Adv. Mater.* **2008**, *20*, 478–483. (b) Lee, S.-M.; Chen, H.; O'Halloran, T. V.; Nguyen, S. T. *J. Am. Chem. Soc.* **2009**, *131*, 9311–9320. (c) Varghese, O. P.; Sun, W. L.; Hilborn, J.; Ossipov, D. *J. Am. Chem. Soc.* **2009**, *131*, 8781–8783. (d) Bryson, J. M.; Fichter, K. M.; Chu, W.-J.; Lee, J.-H.; Li, J.; Madsen, L. A.; McLendon, P. M.; Reineke, T. M. *Proc. Natl. Acad. Sci. U.S.A.* **2009**, *106*, 16913–16918.

(13) Yang, C. S.; Chang, C. H.; Tsai, P. J.; Chen, W. Y.; Tseng, F. G.; Lo, L. W. *Anal. Chem.* **2004**, *76*, 4465–4471.

(14) (a) Wang, L.; Yang, C. Y.; Tan, W. H. *Nano Lett.* **2005**, *5*, 37–43. (b) He, Y.; Su, Y.; yang, X.; Kang, Z.; Xu, T.; Zhang, R.; Fan, C.; Lee, S.-T. *J. Am. Chem. Soc.* **2009**, *131*, 4434–4438.

(15) (a) Michalet, X.; Pinaud, F. F.; Bentolila, L. A.; Tsay, J. M.; Doose, S.; Li, J. J.; Sundaresan, G.; Wu, A. M.; Gambhir, S. S.; Weiss, S. *Science* **2005**, *307*, 538–544. (b) Chan, W. C. W.; Nie, S. M. *Science* **1998**, *281*, 2016–2018. (c) So, M.-K.; Xu, C.; Loening, A. M.; Gambhir, S. S.; Rao, J. *Nat. Biotechnol.* **2006**, *24*, 339–343.

(16) Yang, J.; Zhang, Y.; Gautam, S.; Liu, L.; Dey, J.; Chen, W.; Mason, R. P.; Serrano, C. A.; Schug, K. A.; Tang, L. *Proc. Natl. Acad. Sci. U.S.A.* **2009**, *106*, 10086–10091.

(17) (a) Medintz, I. L.; Clapp, A. R.; Mattoussi, H.; Goldman, E. R.; Fisher, B.; Mauro, J. M. *Nat. Mater.* **2003**, *2*, 630–638. (b) Lee, J. S.; Green, J. J.; Love, K. T.; Sunshine, J.; Langer, R.; Anderson, D. G. *Nano Lett.* **2009**, *9*, 2402–2406. (c) Lewinski, N.; Colvin, V.; Drezek, R. *Small* **2008**, *4*, 26–49.

(18) (a) Wu, C.; Bull, B.; Szymanski, C.; Christensen, K.; McNeill, J. *ACS Nano* **2008**, *2*, 2415–2423. (b) Moon, J. H.; McDaniel, W.; MacLean, P.; Hancock, L. F. *Angew. Chem., Int. Ed.* **2007**, *46*, 8223–8225. (c) Feng, X.; Tang, Y.; Duan, X.; Liu, L.; Wang, S. *J. Mater. Chem.* **2010**; DOI: 10.1039/b915112e.

(19) (a) Thomas, S. W. III; Joly, G. D.; Swager, T. M. *Chem. Rev.* **2007**, *107*, 1339–1386. (b) Liu, B.; Bazan, G. C. *Chem. Mater.* **2004**, *16*, 4467–4476. (c) Ho, H. A.; Najari, A.; Leclerc, M. *Acc. Chem. Res.* **2008**, *41*, 168–178. (d) Achyuthan, K. E.; Bergstedt, T. S.; Chen, L.; Jones, R. M.; Kumaraswamy, S.; Kushon, S. A.; Ley, K. D.; Lu, L.; McBranch, D.; Mukundan, H.; Rininsland, F.; Shi, X.; Xia, W.; Whitten, D. G. *J. Mater. Chem.* **2005**, *15*, 2648–2656. (e) Jiang, H.; Taranekar, P.; Reynolds, J. R.; Schanze, K. S. *Angew. Chem., Int. Ed.* **2009**, *48*, 4300–4316.

(20) (a) Duan, X.; Liu, B.; Feng, F.; Wang, S. *Acc. Chem. Res.* **2009**; DOI: 10.1021/ar9001813. (b) Feng, F.; He, F.; An, L.; Wang, S.; Li, Y.; Zhu, D. *Adv. Mater.* **2008**, *20*, 2959–2964. (c) An, L.; Wang, S. *Chem. Asian J.* **2009**, *4*, 1196–1206.

(21) (a) Sigurdson, C. J.; Nilsson, K. P. R.; Hornemann, S.; Manco, G.; Polymenidou, M.; Schwarz, P.; Leclerc, M.; Hammarström, Per, Wüthrich, K.; Aguzzi, A. *Nat. Methods* **2007**, *4*, 1023–1030. (b) McRae, R. L.; Phillips, R. L.; Kim, I.-B.; Bunz, U. H. F.; Fahrni, C. J. *J. Am. Chem. Soc.* **2008**, *130*, 7851–7853. (c) Björk, Per.; Nilsson, K. P. R.; Lenner, L.; Kågedal, B.; Persson, B.; Inganäs, O.; Jonasson, Jon *Mol. Cell. Probes* **2007**, *21*, 329–337. (d) Li, K.; Pan, J.; Feng, S.-S.; Wu, A. W.; Pu, K.-Y.; Liu, Y.; Liu, B. *Adv. Funct. Mater.* **2009**, *19*, 3535–3542.

(22) (a) Gill, R.; Freeman, R.; Xu, J. P.; Willner, I.; Winograd, S.; Shweky, I.; Banin, U. *J. Am. Chem. Soc.* **2006**, *128*, 15376–15377. (b) Feng, X.; Feng, F.; Yu, M.; He, F.; Xu, Q.; Tang, H.; Wang, S.; Li, Y.; Zhu, D. *Org. Lett.* **2008**, *10*, 5369–5372.

(23) (a) Peng, Z.; Bao, Z.; Galvin, M. E. *Adv. Mater.* **1998**, *10*, 680–684. (b) Lee, K.; Rouillard, J.-M.; Pham, T.; Gulari, E.; Kim, J. *Angew. Chem., Int. Ed.* **2007**, *46*, 4667–4670.

(24) Denizot, F.; Lang, R. *J. Immunol. Methods* **1986**, *89*, 271–277.

(25) Li, C. *Adv. Drug Delivery Rev.* **2002**, *54*, 695–713.

(26) Lakowicz, J. R. *Principles of Fluorescence Spectroscopy*; Kluwer Academic/Plenum: New York, 1999.

(27) Yang, R.; Wu, H.; Cao, Y.; Bazan, G. C. *J. Am. Chem. Soc.* **2006**, *128*, 14422–14423.

(28) Chen, S.-H.; Chen, Y. *Macromolecules* **2005**, *38*, 53–60.

AM100435K